Journal of
Composites Science

MDPI

Article

Exploration of Mechanical and Thermal Properties of CTAB-Modified MoS_2/LLDPE Composites Prepared by Melt Mixing

Suman Chhetri [1,2], Nitai Chandra Adak [1,2], Pranab Samanta [1,2], Naresh Chandra Murmu [1,2] and Tapas Kuila [1,2,*]

1 Surface Engineering & Tribology Division, Council of Scientific and Industrial Research-Central Mechanical Engineering Research Institute (CSIR-CMERI), Durgapur 713209, India; schhetri79@yahoo.com (S.C.); nitaidk3@gmail.com (N.C.A.); ps.iitb@gmail.com (P.S.); ncmurmu@gmail.com (N.C.M.)

2 Academy of Scientific and Innovative Research (AcSIR), CSIR-CMERI, Campus, Durgapur 713209, India

* Correspondence: tkuila@gmail.com; Tel.: +91-9647205077; Fax: +91-343-2548204

Received: 30 May 2018; Accepted: 19 June 2018; Published: 25 June 2018

Abstract: Molybdenum disulfide (MoS_2) was functionalized by cetyltrimethylammonium bromide (CTAB) through a one-pot hydrothermal technique, and subsequently, linear low-density polyethylene (LLDPE) composites were prepared. The attachment of alkyl chains of CTAB onto the MoS_2 surface was confirmed by Fourier transform infrared spectroscopy (FTIR). The enhanced mechanical properties of the composites relative to neat LLDPE revealed good compatibility between MoS_2 and LLDPE. The improvement in thermomechanical properties further substantiated good interaction between MoS_2 and LLDPE. The thermal stability of the prepared composites showed a small decrease in onset degradation temperature. Nevertheless, the char residue formation was found to be promoted in the presence of MoS_2.

Keywords: functionalization; morphology; mechanical properties; glass transition temperature

1. Introduction

The discovery of graphene and its subsequent surge in the academic and industrial spheres inspired researchers to excavate other 2-D materials, such as transition metal dichalcogenides, hexagonal boron nitride, carbon nitride (C_3N_4), and so forth. [1]. Among these, molybdenum disulfide (MoS_2), with a structure akin to graphene, has attracted significant attention in different fields, which arises mainly from its 2-D morphology, atomic thickness, and semiconductor characteristics. Thus, 2-D layered MoS_2 has been widely studied in the fields such as catalysis, supercapacitors, transistors, lithium ion batteries, and polymer nanocomposites [2–9]. The 2-D layered MoS_2 possesses high modulus of ~300 GPa and has proven to be a very efficient filler in reinforcing polymer matrices [10,11]. In recent times, MoS_2 has been used as a reinforcement filler in polymer matrices such as polyethylene, poly(vinylalcohol), epoxy, polystyrene, methyl methacrylate, chitosan, polyurethane, nylon, polyamide, methylcellulose, and so forth, and significant enhancements in mechanical, thermal, tribological, and fire resistance properties have been recorded with small weight fractions of MoS_2 [9,11–20]. Among the 2-D reinforcing filler, graphene has been widely used and has found wide acceptance in the scientific and industrial realms [21]. Although graphene could produce mechanically robust and thermally stable high-performance composites, being electrically conducting in nature, it may also impart electrical conductivity to the host matrix, thereby restricting its uses in areas such as electronic packaging, electric motors, transmission lines, and so forth [11]. In the aforementioned applications, it is necessary to enhance mechanical properties and thermal stability of the composite materials while preserving the insulating properties of the host polymer materials.

Because of its semiconductor characteristics, MoS_2 does not endow electrical conductivity to the host polymer matrix, so MoS_2-based polymer composites may be befitting alternatives to conducting graphene-based composites.

The exciting properties of MoS_2 nanosheets are associated with its 2-D morphology and its atomic thickness. However, in order to transfer the intrinsic properties of MoS_2 into a polymer matrix, homogenous dispersion and distribution of MoS_2 is very crucial. The extent of interfacial interaction/adhesion between a polymer matrix and filler is strongly dependent on the degree of dispersion of filler particles [22–24]. Anchoring organic moieties onto the surface of MoS_2 could be one of the plausible ways to improve the interaction, compatibility, and dispersion of MoS_2 in organic polymer systems. Hence, the preparation of mono- or multilayer MoS_2 and its functionalization is crucial to realize the full reinforcing potential. Many prior reports used functionalized MoS_2 nanosheets to reinforce the polymer matrix, and it has been observed that suitably tuned MoS_2 nanosheets could endow significant enhancement in mechanical, thermal, and other properties [11–18]. Feng et al. used dodecanethiol as an antioxidant and surface modifier to produce defect-free MoS_2 by direct ultrasonication of bulk MoS_2 and prepared the polyethylene nanocomposites by incorporating defect-free modified MoS_2 [9]. The study revealed improved mechanical and thermal properties upon incorporation of MoS_2. Typically, solution-based exfoliation techniques are employed to generate MoS_2 nanosheets. The exfoliation-based technique consumes large amount of organic solvents and requires prolonged sonication, which may deform the MoS_2 structure and create defects. So, concurrent preparation and functionalization of MoS_2 through a one-pot method could be one of the effective ways to achieve defect-free MoS_2 sheets. The intent of this work is to shed light on the effect of functionalized MoS_2 sheets on the mechanical and thermal properties of linear low-density polyethylene (LLDPE) composites prepared through an industrially viable melt-mixing process.

Herein, the cetyltrimethylammonium bromide (CTAB)-assisted hydrothermal synthesis of MoS_2 (denoted as CTAB–MoS_2) and the subsequent fabrication of CTAB–MoS_2/LLDPE composites by melt mixing has been reported. It is expected that the CTAB surfactant shall be adsorbed electrostatically onto the surface of the anionic precursor (MoO_4^{2-}) formed during the synthesis of MoS_2 and assist in the formation of mono- or multilayer MoS_2 particles, and additionally, help to inhibit the restacking or agglomeration of MoS_2 layers. LLDPE, one of the widely used thermoplastic polymers, has been selected as the polymer matrix. LLDPE has enormous applications, mainly for plastic films, tubes, and so forth, due to its excellent tear resistance and impact strength, large elongation, and excellent puncture resistance [25,26]. However, pure LLDPE suffers from certain limitations such as low mechanical properties and low thermal resistance, amongst others. A melt-mixing technique was employed to fabricate the composites and it may be considered advantageous over solution mixing, as this technique is devoid of the use of hazardous solvents.

2. Materials and Methods

2.1. Materials

Sodium molybdate (Na_2MoO_4) and thiourea (CH_4N_2S) were purchased from Merck, Mumbai, India. Cetyltrimethylammonium bromide (CTAB) was purchased from Himedia, Mumbai, India. LLDPE polymer pellets were supplied by Reliance Industries Limited, Jamnagar, Gujarat, India. All the reagents were of analytical grade and used as received without further purification.

2.2. CTAB Assisted Synthesis of MoS_2

The CTAB-embedded MoS_2 nanosheets were prepared by a facile hydrothermal route as reported in our earlier work [18]. Typically, ~1.2 g of $Na_2MoO_4 \cdot 2H_2O$ and 3.2 g of CH_4N_2S were dissolved in 60 mL of distilled water. After that, 3 g of CTAB was dissolved into the mixture under stirring to form a homogenous solution. The clear solution was then introduced into a 100 mL Teflon-lined stainless steel autoclave and maintained at 180 °C for 16 h. Then, the autoclave was allowed to cool to room

temperature. The black precipitates so formed were collected by centrifugation, followed by washing with distilled water and absolute ethanol. The final product was dried in a vacuum oven at 80 °C for 12 h and designated as CTAB–MoS_2. The pristine MoS_2 was prepared following the similar procedure, albeit without using CTAB.

2.3. Preparation of CTAB–MoS2/LLDPE Composites

LLDPE composites of different weight fractions of CTAB–MoS_2 were prepared by melt compounding on a Sigma melt mixer (S.C. Dey Co., Kolkata, India), at a processing temperature of 125 °C, screw speed of 60 rpm, and the mixing time of 15 min. The melt mixing was conducted by initially adding the polymer slowly into the mixing compartment. When the polymer melted completely, CTAB–MoS_2 was added to the molten polymer. The material obtained after melt mixing was cooled to room temperature and collected as lumps. It was then hot-pressed into a sheet of thickness ~2 mm on an electrically heated hydraulic press. The pallets were held for ~15 min in the hot-pressing machine at a temperature of 150 °C. After cooling to room temperature, the samples were cut into different dimensions from the sheet for performing various tests. Figure 1 shows the schematic of the functionalization of MoS_2 with CTAB and preparation of its composites with LLDPE matrix by melt mixing.

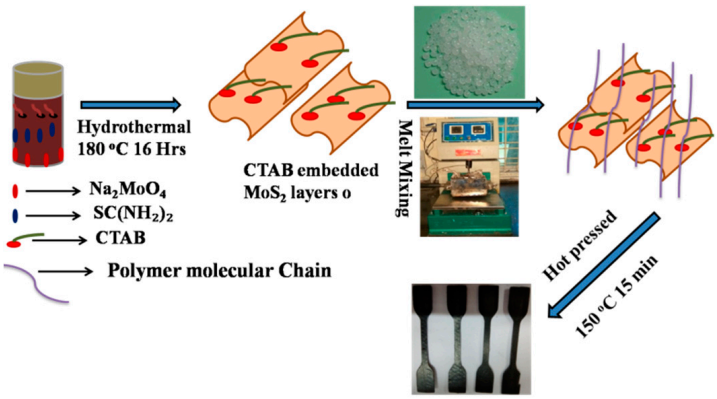

Figure 1. Schematic for the functionalization of MoS_2 by cetyltrimethylammonium bromide (CTAB) and preparation of linear low-density polyethylene (LLDPE) composites by melt mixing.

2.4. Characterization

The functionalization of MoS_2 was confirmed by Fourier transform infrared (FT-IR) spectra. FT-IR spectra were recorded with a Perkin Elmer RXI FT-IR (PerkinElmer, Inc., Waltham, MA, USA) in the range of 4000–400 cm^{-1}. The formation of MoS_2, CTAB–MoS_2, and exfoliation of functionalized MoS_2 in LLDPE were confirmed by X-ray diffraction (XRD). XRD was performed in PANalytical (Model X pert PRO) at a scan rate of 0.106° s^{-1} in between the 2θ range of 5–60°. Field emission scanning electron microscopy (FE-SEM)was performed using ∑igma HD, Carl Zeiss, Germany, to study the morphology of the CTAB–MoS_2/LLDP composite fracture sample. The dispersion of functionalized MoS_2 in the LLDPE matrix was studied by transmission electron microscopy (TEM) with a JEOLTEM 2100 FS instrument (JEOL Ltd., Tokyo, Japan) at 200 kV. The ultrathin TEM sample of thickness ~70 nm of the composites was cut using a Leica Ultracut UCT (Leica Microsystems Inc., Buffalo Grove, IL, USA) ultramicrotome at room temperature. Microtomed composite samples were then collected over copper grids for TEM observation. The tensile measurements were performed using a Tinius Olsen h50KS (Tinius Olsen, Horsham, PA, USA) universal testing machine at 25 °C with a crosshead speed of 1 mm·min^{-1} according to ASTMD-638 standard. The sample dimension was 77 mm in length (working length 26 mm), 5 mm in width, and 1.5–2 mm in thickness. The values were taken as the average of three specimens. Dynamic mechanical analysis (DMA) was conducted in a Perkin

Elmer DMA 8000 in the temperature range of −80 to 90 °C. The heating rate was 3 °C min^{-1} and the frequency and load strain were 1 Hz and 0.10 mm, respectively. Rectangular specimens of dimension 9mm × 9.6 mm × 2.2 mm were prepared for DMA measurements. Thermogravimetric analysis (TGA) was performed in a Jupiter STA 449 F1 (Netzsch, Germany) thermal analyser to study the thermal stability of the composites. The samples (~5.56 mg) were heated from 30 °C to 750 °C at a heating rate of 5 °C·min^{-1} in an air atmosphere.

3. Results and Discussion

3.1. Characterization of MoS_2 and CTAB–MoS_2

In order to confirm the functionalization of MoS_2 by long alkyl chain CTAB, FT-IR spectra analysis was performed. Figure 2a shows the FT-IR spectra of pure MoS_2 and CTAB–MoS_2; the two peaks observed for CTAB–MoS_2 at 2923 and 2853 cm^{-1} can be assigned to the C–H stretching vibrations of –CH_3 and –CH_2 groups present in CTAB, which are absent in pure MoS_2 prepared by a similar type of hydrothermal method. The appearance of peaks at 1459 and 712 cm^{-1}, attributed to the asymmetric and bending δ_{C-H} vibrations of –CH_3 and –CH_2, further validated the presence of long alkyl chains [27]. To further confirm the modification of MoS_2 by CTAB, XRD was performed for CTAB–MoS_2 and pristine MoS_2, and the corresponding reflection plane are shown in Figure 2b. For pristine MoS_2, an intense reflection peak at 2θ = 14.48° (corresponding to the interlayer distance of 0.62 nm) was observed, which was ascribed to the (002) reflection plane [18]. In contrast, the (002) peak of CTAB–MoS_2 shifted to a lower 2θ (~7.5°). The shifting of the (002) peak towards a lower angle signifies that CTAB was successfully intercalated and attached on to the MoS_2 nanolayers, which led to enlargement of the interlayer spacing. The enlargement in interlayer spacing is considered to be advantageous for composite preparation as it would facilitate the intercalation of polymer within the gallery of 2D materials, thus leading to a robust interface.

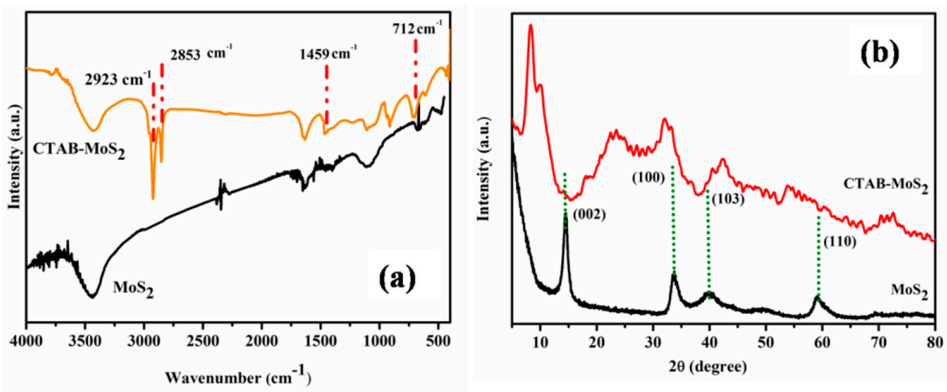

Figure 2. (**a**) FT-IR spectra for MoS_2 and CTAB–MoS_2 and (**b**) X-ray diffraction (XRD) pattern of MoS_2 and CTAB–MoS_2.

Figure 3a,b depicts the overview of the morphologies of pristine MoS_2 and CTAB–MoS_2. Figure 3a shows the highly ordered tightly stacked FE-SEM image of hydrothermally prepared pristine MoS_2. Upon functionlization, the highly ordered structure of MoS_2 was found to be disturbed as shown in Figure 3b. The red arrows (Figure 3b) point to the separated layers of MoS_2 particles. It was expected that CTAB assisted in the growth of multilayer MoS_2 particles.

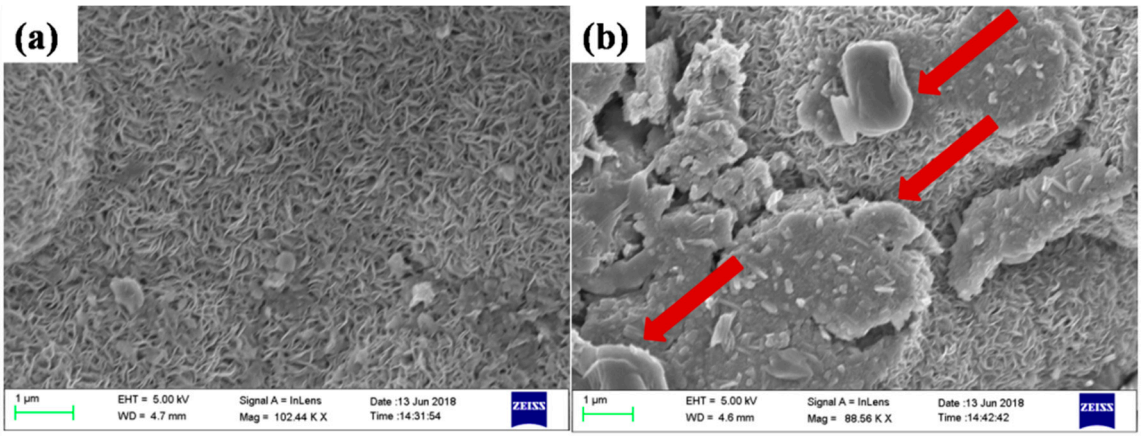

Figure 3. Field emission scanning electron microscopy (FE-SEM) micrographs of (**a**) pristine MoS_2 (**b**) and CTAB–MoS_2.

3.2. Stress–Strain Behaviour Analysis

The optimum reinforcing potential of the layered structured filler can only be realized if efficient stress transfer takes place across the polymer–filler interface. Thus, homogenous dispersion in tandem with strong interfacial interaction between the filler and polymer matrix should be ensured. Tensile testing was carried out to evaluate the effect of CTAB–MoS_2 on the mechanical properties of LLDPE. Figure 4a displays the typical stress–strain curves of pure LLDPE and its composites with different content of CTAB–MoS_2. The composites showed enhanced tensile strength and a maximum improvement of 35% in tensile strength containing 2 wt % of CTAB–MoS_2 loading. The improvement in tensile strength revealed the good reinforcing competency of MoS_2. The modification of MoS_2 with the moiety bearing long alkyl chains improved its good interfacial interaction with the LLDPE matrix, which in turn leads to the creation of strong junction cohesion suitable for efficient stress transfer across the interface. It is assumed that the long alkyl chains of the surfactant attached to MoS_2 might have developed hydrophobic affinity with LLDPE matrix, leading to the robust interface. The Young's modulus for various LLDPE/CTAB–MoS_2 composites derived from stress–strain curves are shown in Figure 4b. The LLDPE/CTAB–MoS_2 composites containing 2 wt % CTAB–MoS_2 showed highest improvement among the studied composites. An improvement of ~43.5% was recorded against neat LLDP, which was ascribed to the stiffness and physical structure of MoS_2 particles.

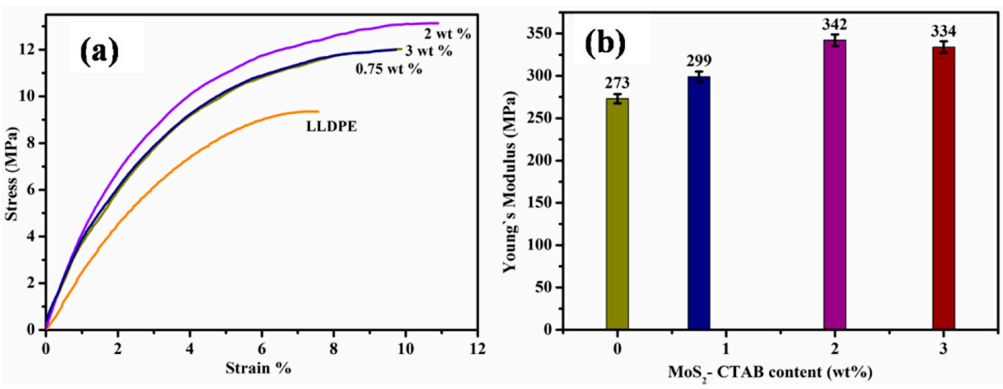

Figure 4. Stress–strain curve of neat LLDPE and its composites with CTAB–MoS_2 at various loadings (**a**) and variation of Young's modulus with weight percentage of CTAB–MoS_2 (**b**).

3.3. Morphological and Structural Investigation

FE-SEM images of the tensile fractured sample were used to study the variations in the micro-morphology of the fracture surface of pure LLDPE and its composite with CTAB–MoS_2. The different-magnification images of the fractured morphology of pure LLDPE and composites have been presented in Figure 5a–d. Subtle investigation of the FE-SEM images of pure LLDPE and composites exhibited variations in their surface morphologies. The neat LLDPE showed a comparatively smooth fracture surface, which signifies that the failure of the material took place at lower stress. On the contrary, the fracture surface of LLDPE composites displayed rough surfaces, which indicates improved resistance of the materials against load. The appearance of a pulled thread-like morphology confirms the strong interfacial interactions between MoS_2 and the LLDPE matrix, which accounts for the improved mechanical properties.

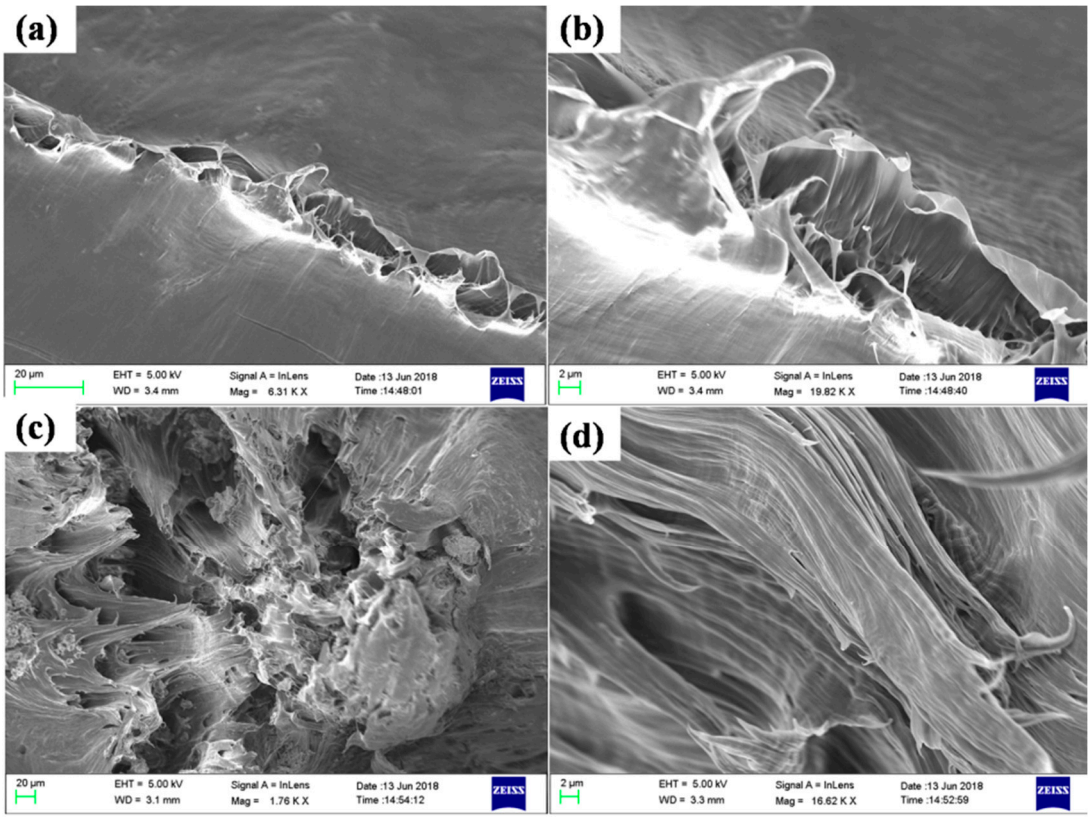

Figure 5. FE-SEM images of the tensile fractured surface of (**a**,**b**) neat epoxy and (**c**,**d**) CTAB–MoS_2 (2 wt %)/LLDPE composite.

X-ray diffraction is helpful to comprehend the degree of exfoliation of the filler in the polymer matrix. Figure 6 shows the X-ray diffraction patterns of pure LLDPE and CTAB–MoS_2/LLDPE composites. The XRD pattern of pure LLDPE exhibited two main peaks at 2θ~21.49° and 23.75°, corresponding to the (110) and (200) planes, respectively [28]. As the loading of the CTAB–MoS_2 increased, the peaks at 2θ~21.49° and 23.75° for LLDPE were found to increase. However, no peaks corresponding to MoS_2 were observed, thus indicating the complete exfoliation and distribution of MoS_2 in the LLDPE composites. TEM micrographs of the composites demonstrate the intricate nature of the morphology of the dispersed MoS_2 nanosheets. As can be seen from the TEM micrograph, complete exfoliations of MoS_2 nanosheets are hardly observed. However, the diffused nature of the MoS_2 nanosheets is observed in Figure 7.

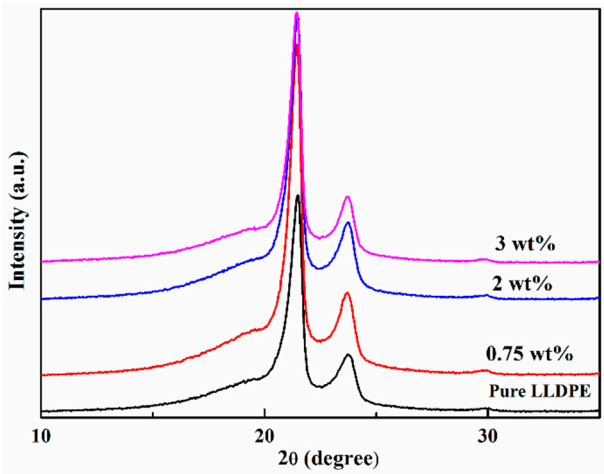

Figure 6. XRD pattern of CTAB–MoS_2/LLDPE composites at various weight fractions.

The regions with highly concentrated MoS_2 nanosheets are distinguished from the regions of low concentration of MoS_2 nanosheets. The phase separation may also be due to the high stress induced by the diamond knife during sample preparation by ultramicrotomy [29]. The TEM images did not reveal the sheet-like morphology of MoS_2, which may be due to the low concentration of exfoliated MoS_2 nanosheets. However, the dark areas are certainly generated due to the small thickness of debonded MoS_2 nanosheets.

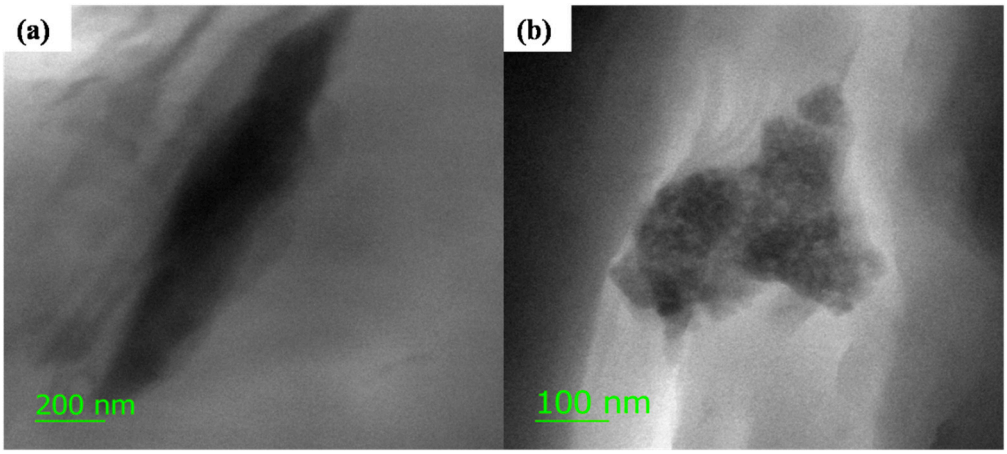

Figure 7. TEM micrograph of (**a**,**b**) CTAB–MoS_2/LLDPE composite with 2 wt %CTAB–MoS_2.

3.4. Dynamic Mechanical Analysis

DMA is a powerful investigation technique to study the interfacial interaction between the filler material and polymer matrix. DMA studies are sensitive to filler matrix interaction and the segmental motion of the polymer chains at the filler–matrix interfaces. The DMA were studied to quantify the mobility of the polymeric segments and to understand the interphase properties of pure epoxy and its composites with CTAB–MoS_2. The results investigated in terms of storage modulus (E′), loss modulus (E″), and tan δ (loss factor) are shown in Figure 8a, Figure 8b, and Figure 8c, respectively. The dynamic mechanical properties of neat LLDPE and its composites were evaluated within the temperature range of −80 °C to 90°C. Figure 7a shows the temperature dependence of the storage modulus, E′, and the corresponding values are summarized in Table 1. It quantifies the energy storing ability of the material under load. The E′ value of the composites was found to be higher than those of neat LLDPE, irrespective of the range of temperature under study. The maximum enhancement of ~79% in

the storage modulus of LLDPE/CTAB–MoS_2 composites was recorded at 2 wt % of CTAB–MoS_2. This indicated improved stiffness and restricted mobility of the polymeric chains. The significantly improved modulus suggested obstruction in the movements of polymer chains by firmly embedded CTAB–MoS_2. Furthermore, the improvement of the storage modulus in the solid state can be correlated with the improved mechanical properties and impact strength of the composites. It means that incorporation of CTAB–MoS_2 enhanced the impact resistance of LLDPE composites. It was assumed that the presence of the hydrophobic long alkyl chains in CTAB–MoS_2 played a crucial role in enhancing the compatibility of MoS_2 within the LLDPE matrix, which ameliorated the interaction between the two constituents, thereby inhibiting the segmental motion of the polymer chains.

Table 1. Storage modulus, E′, of neat LLDPE and its composites at different temperatures.

Sample Code	E′ (MPa) −78 °C	E′ (MPa) −50 °C	E′ (MPa) 5 °C	E′ (MPa) 60 °C
Pure LLDPE	1560	1291	632	**250**
0.75 wt %	2444	2117	1059	**401**
2 wt %	2797	2362	1167	**451**
3 wt %	1345	2025	979	**371**

Figure 8b shows the variation of tan δ (E″/E′) and the loss modulus (E″) of the CTAB-MoS_2/LLDPE composites with temperature. The glass transition temperature (T_g) of the polymer composite system can be deduced from the peak position of the tan δ (E″/E′) curve. However, at times, it becomes difficult to derive the exact maxima value due to the elusive nature of the curves [30]. In such instances, the peak position of the E″ curve could be assumed as the probable T_g of the polymer matrix in the composites. The E'' value signifies the quantity of unrecoverable energy dissipation per cycle, and it was found to increase upon the incorporation of CTAB–MoS_2, which may be ascribed to the increase in friction between the MoS_2 and LLDPE matrix.

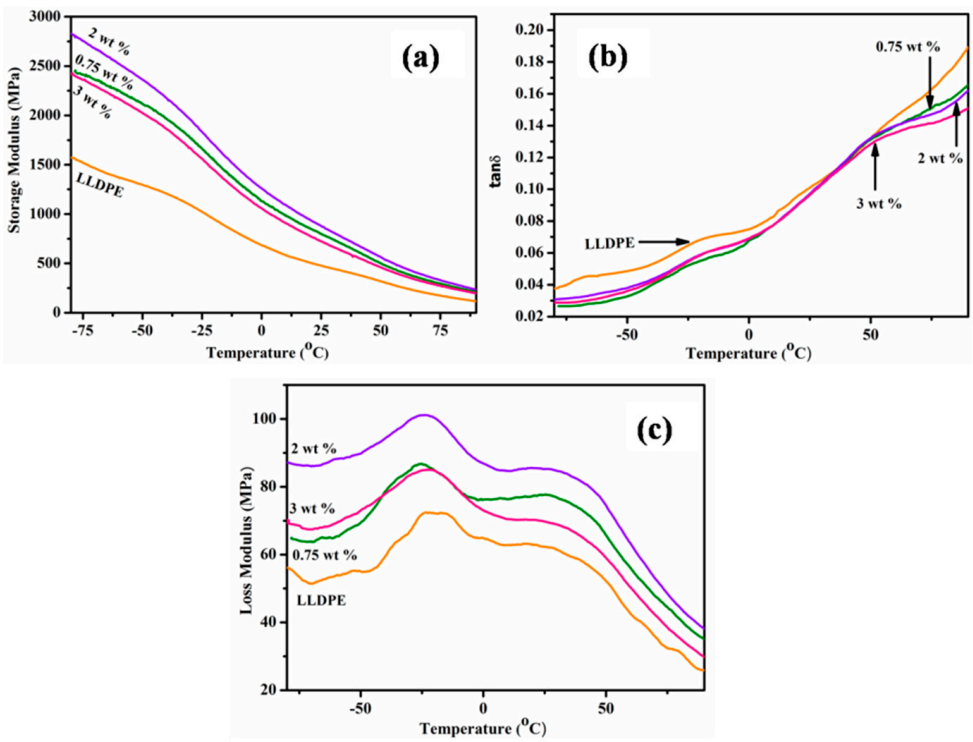

Figure 8. Variation of storage modulus (E′) with temperature (**a**), variation of tan δ with temperature (**b**), and variation of loss modulus (E″) with temperature for CTAB–MoS_2/LLDPE composites (**c**).

3.5. Thermogravimetric Analysis

The thermal degradation behaviour of LLDPE and its composites were investigated by TGA. The TGA thermograms of LLDPE and CTAB–MoS_2/LLDPE composites performed under air atmosphere are shown in Figure 9. The initial decomposition of CTAB–MoS_2/LLDPE composites, which was evaluated from the temperatures corresponding to 5 and 10 wt % weight loss ($T_{-5\%}$ and $T_{-10\%}$) was found to be decreased as compared to pure LLDPE. The onset degradation temperature of the composites was further found to decrease with the increased in the loading of CTAB–MoS_2. When the content of CTAB–MoS_2 was increased to 3.0 wt %, the temperature corresponding to 5.0 wt % mass loss ($T_{-5\%}$) was decreased by ~20 °C as compared to that of pure LLDPE. The reduction in onset degradation temperature could be ascribed to the decomposition of the CTAB and to the high thermal conductivity of MoS_2, which could have assisted in the easy delivery of heat. The char formation during thermal decomposition of the materials is a crucial parameter to judge the materials' competency in real-life applications. The char residue was found to be promoted in the presence of CTAB–MoS_2; the char residue until 750 °C for all the composites showed an increase as compared to pure LLDPE (as shown in the inset of Figure 9). Thus, CTAB–MoS_2 could have acted as a catalyst to promote the formation of the char residue during degradation [16,31]. In addition, the presence of inorganic MoS_2 contributed to the formation of char residue, due to its nondegradable nature. The formation of a char is expected to impede the out-diffusion of the decomposed products by forming a protective layer, which consequently promotes the thermal stability of the composites.

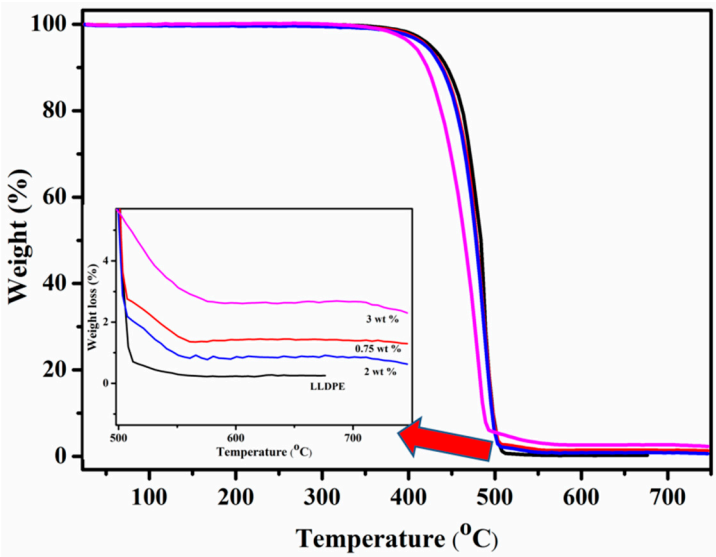

Figure 9. Thermogravimetric analysis (TGA) curves of CTAB–MoS_2/LLDPE composites.

4. Conclusions

Motivated by the wide array of applications of graphene, in this study, 2-D layered structure MoS_2 was explored as a filler for a LLDPE matrix. Surfactant CTAB was used to assist the preparation of exfoliated MoS_2 and also as modifier. CTAB–MoS_2/LLDPE composites were prepared following an industrially viable and environment friendly melt-mixing technique. FT-IR spectra analysis was used to confirm the embedment of CTAB on the surface of MoS_2. The presence of long alkyl chains helped to generate strong junction cohesion, which was reflected by the improvement of mechanical properties. The tensile strength of the composites was found to improve by ~35% at 2 wt % of CTAB–MoS_2 loadings. The substantial improvement in the storage modulus value confirmed the role of CTAB in improving the interfacial interaction of MoS_2 within the LLDPE matrix. A maximum improvement of ~79% in the storage modulus at the loading of 2 wt % was recorded. The improved storage modulus signified the superior interfacial interaction between the modified MoS_2 and LLDPE

matrix. The thermal stability of the CTAB–MoS_2/LLDPE composites investigated by TGA showed a small decrease in the onset degradation temperature. Nevertheless, the char residue formation was found to improve in the presence of MoS_2. Although the improvements in the end properties of the polymer composites might be lessened when processed by melt mixing, as compared to solution mixing, this simple strategy may be promising for developing mechanically strong composites.

Author Contributions: T.K. designed and coordinated the research work. N.C.A. and S.C. performed all the experiments. N.C.M. and P.S. analyzed the mechanical testing of the developed materials. All the authors assisted in the assembly and editing of the manuscript.

Funding: This research was funded by Department of Science and Technology, New Delhi, India grant number [GAP211412].

Acknowledgments: Authors are thankful to the Director of Council of Scientific and Industrial Research-Central Mechanical Engineering Research Institute (CSIR-CMERI).

Conflicts of Interest: The authors declare no conflict of interest.

References

1. Rao, C.N.R.; Maitra, U.; Waghmare, U.V. Extraordinary attributes of 2-dimensional MoS_2 nanosheets. *Chem. Phys. Lett.* **2014**, *609*, 172–183. [CrossRef]
2. Benck, J.D.; Chen, Z.; Kuritzky, L.Y.; Forman, A.J.; Jaramillo, T.F. Amorphous molybdenum sulfide catalysts for electrochemical hydrogen production: insights into the origin of their catalytic activity. *ACS Catal.* **2012**, *2*, 1916–1923. [CrossRef]
3. Merki, D.; Hu, X. Recent developments of molybdenum and tungsten sulfides as hydrogen evolution catalysts. *Energy Environ. Sci.* **2011**, *4*, 3878–3888. [CrossRef]
4. Ma, G.; Peng, H.; Mu, J.; Huang, H.; Zhou, X.; Lei, Z. In situ intercalative polymerization of pyrrole in graphene analogue of MoS_2 as advanced electrode material in supercapacitor. *J. Power Sources* **2013**, *229*, 72–78. [CrossRef]
5. Ramadoss, A.; Kim, T.; Kim, G.S.; Kim, S.J. Enhanced activity of a hydrothermally synthesized mesoporous MoS_2 nanostructure for high performance supercapacitor applications. *New J. Chem.* **2014**, *38*, 2379–2385. [CrossRef]
6. Wang, Z.; Chen, T.; Chen, W.; Chang, K.; Ma, L.; Huang, G.; Chen, D.; Lee, J.Y. CTAB-assisted synthesis of single-layer MoS_2–graphene composites as anode materials of Li-ion batteries. *J. Mater. Chem. A* **2013**, *1*, 2202–2210. [CrossRef]
7. Li, H.; Yu, K.; Fu, H.; Guo, B.; Lei, X.; Zhu, Z. MoS_2/graphene hybrid nano flowers with enhanced electrochemical performances as anode for lithium-ion batteries. *J. Phys. Chem. C* **2015**, *119*, 7959–7968. [CrossRef]
8. Radisavljevic, B.; Radenovic, A.; Brivio, J.; Giacometti, V.; Kis, A. Single-layer MoS_2 transistors. *Nat. Nanotechnol.* **2011**, *6*, 147–150. [CrossRef] [PubMed]
9. Feng, X.; Wena, P.; Cheng, Y.; Liua, L.; Tai, Q.; Hu, Y.; Liew, K.M. Defect-free MoS_2 nanosheets: Advanced nanofillers for polymer nanocomposites. *Compos. Part A: Appl. Sci. Manuf.* **2016**, *81*, 61–68. [CrossRef]
10. Castellanos-Gomez, A.; Poot, M.; Steele, G.A.; van der Zant, H.S.J.; Agrait, N.; Rubio-Bollinger, G. Elastic properties of freely suspended MoS_2 nanosheets. *Adv. Mater.* **2012**, *24*, 772–775. [CrossRef] [PubMed]
11. Eksik, O.; Gao, J.; Shojaee, S.A.; Thomas, A.; Chow, P.; Bartolucci, S.F.; Lucca, D.A.; Koratkar, N. Epoxy nanocomposites with two-dimensional transition metal dichalcogenide additives. *ACS Nano* **2014**, *8*, 5282–5289. [CrossRef] [PubMed]
12. Zhou, K.; Jiang, S.; Bao, C.; Song, L.; Wang, B.; Tang, G.; Hu, Y.; Gui, Z. Preparation of poly(vinyl alcohol) nanocomposites with molybdenum disulfide (MoS_2): Structural characteristics and markedly enhanced properties. *RSC Adv.* **2012**, *2*, 11695–11703. [CrossRef]
13. Zhou, K.; Jiang, S.; Shi, Y.; Liu, J.; Wang, B.; Hu, Y.; Gui, Z. Multigram-scale fabrication of organic modified MoS2 nanosheets dispersed in polystyrene with improved thermal stability, fire resistance, and smoke suppression properties. *RSC Adv.* **2014**, *4*, 40170–40180. [CrossRef]

14. Zhou, K.; Liu, J.; Wang, B.; Zhang, Q.; Shi, Y.; Jiang, S.; Hu, Y.; Gui, Z. Facile preparation of poly (methylmethacrylate)/MoS_2 nanocomposites via in situ emulsion polymerization. *Mater. Lett.* **2014**, *126*, 159–161. [CrossRef]
15. Wang, X.; Xing, W.; Feng, X.; Yu, B.; Song, L.; Yeoh, G.H.; Hu, Y. Enhanced mechanical and barrier properties of polyurethane nanocomposite films with randomly distributed molybdenum disulfide nanosheets. *Compos. Sci. Technol.* **2016**, *127*, 142–148. [CrossRef]
16. Zhou, K.; Liu, J.; Zeng, W.; Hu, Y.; Gui, Z. In situ synthesis, morphology, and fundamental properties of polymer/MoS_2 nanocomposites. *Compos. Sci. Technol.* **2015**, *107*, 120–128. [CrossRef]
17. Yang, X.; Meng, N.; Zhu, Y.; Zhou, Y.; Nie, W.; Chen, P. Greatly improved mechanical and thermal properties of chitosan by carboxyl-functionalized MoS_2 nanosheets. *J. Mater. Sci.* **2016**, *51*, 1344–1353. [CrossRef]
18. Chhetri, S.; Adak, N.C.; Samanta, P.; Mandal, N.; Kuila, T.; Murmu, N.C. Investigation of mechanical and thermal properties of the cetyltrimethylammonium bromide functionalized molybdenum disulfide (MoS_2)/epoxy composites. *Polym. Bull.* **2018**, *75*, 327–343. [CrossRef]
19. Tang, G.; Huang, W.; Chang, D.; Nie, W.; Mi, W.; Yan, W. The friction and wear of aramid fiber-reinforced polyamide 6 composites filled with nano-MoS_2. *Polym. Plast. Technol. Eng.* **2011**, *50*, 1537–1540. [CrossRef]
20. Xing, Y.; Zhang, G.; Ma, K.; Chen, T.; Zhao, X. Study on the friction and wear behaviors of modified PA66 composites. *Polym. Plast. Technol. Eng.* **2009**, *48*, 633–638. [CrossRef]
21. Kuila, T.; Bhadra, S.; Yao, D.; Kim, N.H.; Bose, S.; Lee, J.H. Recent advances in graphene based polymer composites. *Prog. Polym. Sci.* **2010**, *35*, 1350–1375. [CrossRef]
22. Wang, K.; Pasbakhsh, P.; De Silva, R.T.; Goh, K.L. A Comparative analysis of the reinforcing efficiency of silsesquioxane nanoparticles versus apatite nanoparticles in chitosan biocomposite fibres. *J. Compos. Sci.* **2017**, *1*, 9. [CrossRef]
23. Bertolino, V.; Cavallaro, G.; Lazzara, G.; Merli, M.; Milioto, S.; Parisi, F.; Sciascia, L. Effect of the biopolymer charge and the nanoclay morphology on nanocomposite materials. *Ind. Eng. Chem. Res.* **2016**, *55*, 7373–7380. [CrossRef]
24. Makaremi, M.; Pasbakhsh, P.; Cavallaro, G.; Lazzara, G.; Aw, Y.K.; Lee, S.M.; Milioto, S. Effect of morphology and size of halloysite nanotubes on functional pectin bionanocomposites for food packaging applications. *ACS Appl. Mater. Interfaces* **2017**, *9*, 17476–17488. [CrossRef] [PubMed]
25. Lu, J.; Sue, H.J. Morphology and mechanical properties of blown films of a low-density polyethylene/linear low-density polyethylene. *J. Polym. Sci. Part B Polym. Phys.* **2002**, *40*, 507–518. [CrossRef]
26. Niaounakis, M.; Kontou, E. Effect of LDPE on the thermo-mechanical properties of LLDPE-based films. *J. Polym. Sci. Part B Polym. Phys.* **2005**, *43*, 1712–1727. [CrossRef]
27. Huang, G.; Chen, T.; Chen, W.; Wang, Z.; Chang, K.; Ma, L.; Huang, F.; Chen, D.; Lee, J.Y. Graphene-like MoS_2/graphene composites: Cationic surfactant-assisted hydrothermal synthesis and electrochemical reversible storage of lithium. *Small* **2013**, *9*, 3693–3703. [CrossRef] [PubMed]
28. Zhao, H.; Lei, Z.; Wang, Z.; Huang, B. Studies on blends of LLDPE and ethylene-methacrylic acid random copolymer. *Eur. Polym. J.* **1999**, *35*, 355–360. [CrossRef]
29. Tang, L.C.; Wan, Y.J.; Yan, D.; Pei, Y.B.; Zhao, L.; Li, Y.B.; Wu, L.B.; Jiang, J.X.; Lai, G.Q. The effect of graphene dispersion on the mechanical properties of graphene/epoxy composites. *Carbon* **2013**, *60*, 16–27. [CrossRef]
30. Kim, S.; Do, I.; Drzal, L.T. Thermal stability and dynamic mechanical behavior of exfoliated graphite nanoplatelets-LLDPE nanocomposites. *Polym. Compos.* **2010**, *31*, 755–761. [CrossRef]
31. Cai, W.; Zhan, J.; Feng, X.; Yuan, B.; Liu, J.; Hu, W.; Hu, Y. Facile construction of flame-retardant-wrapped molybdenum disulfide nanosheets for properties enhancement of thermoplastic polyurethane. *Ind. Eng. Chem. Res.* **2017**, *56*, 7229–7238. [CrossRef]